Forestry An International Journal of Forest Research

Institute of Chartered Foresters

Forestry 2021; 1–11, https://doi.org/10.1093/forestry/cpab034

Estimation of forest canopy structure and understory light using spherical panorama images from smartphone photography

A. Z. Andis Arietta*

Yale School of the Environment, Yale University, 370 Prospect Street, New Haven, CT 06511, USA

*Corresponding author: Email: a.andis@yale.edu

Received 18 December 2020

Accurate estimates of forest canopy structure are central for a wide range of ecological studies. Hemispherical photography (HP) is a popular tool to estimate canopy attributes. However, traditional HP methods require expensive equipment, are sensitive to exposure settings, and produce limited resolution which dramatically affects the accuracy of gap fraction estimates. As an alternative, hemispherical images can be extracted from spherical panoramas produced by many smartphone camera applications. I compared hemispherical photos captured with a digital single lens reflex camera and 180° lens to those extracted from smartphone spherical panoramas (SSP). The SSP HP method leverages built-in features of current generation smartphones to produce sharper images of higher resolution, resulting in more definition of fine canopy structure. Canopy openness and global site factor from SSP HP are highly correlated with traditional methods ($R^2 > 0.9$), while leaf area index estimates are lower, especially in more closed canopies where traditional methods fail to capture fine gaps.

Introduction

Ecological patterns and processes in forests are mediated by the canopy in critical ways (Parker *et al.* 1995). The structure of the canopy directly alters the below-canopy light regime and microclimate which indirectly impacts microhabitat features such as soil moisture, snowpack and understory plant community (Jennings *et al.* 1999). Because of its fundamental importance, forest managers and ecologists alike require methods to accurately quantify canopy structure and light environments.

In recent decades, hemispherical photography (HP), and especially digital HP, has arisen as the most popular optical method for indirectly estimating canopy structure, primed by advances in digital photography equipment and software for image analysis and its relatively lower cost compared to other methods (e.g. laser scanning) (Promis 2013; Yan *et al.* 2019; Chianucci 2020). This technique uses extreme wide-angle lenses with a field-of-view of 180° that projects an entire hemisphere of view onto the camera sensor, resulting in a circular hemispherical image (Rich 1990). Pixels within the image are then classified into binary sky (white) or canopy elements (black) manually or algorithmically using global or local thresholds (Glatthorn and Beckschäfer 2014). From the binarized images, canopy structure measures such as gap fraction, canopy openness (CO), leaf area index (LAI), etc. can be estimated (Frazer *et al.* 1997; Gonsamo *et al.* 2013; Chianucci 2020). By plotting a sun path onto the binarized image, the canopy structure can be used to infer understory light regimes, or Site Factors, given estimates of prevailing above-canopy direct and diffuse radiation (Anderson 1964). Light values can be integrated over time to yield seasonal estimates of light environments from a single sampling event (Frazer *et al.* 1997) (or at least two samples in deciduous canopies (e.g. Halverson *et al.* 2003)). Thus, HP offers an efficient, non-destructive method of estimating forest microhabitat features.

However, HP suffers from methodological drawbacks relating to the difficulty of capturing images in field settings and the sensitivity of estimates to variation in image acquisition (Beckschäfer *et al.* 2013; Bianchi *et al.* 2017). Traditionally, HP requires a single lens reflex camera (or more commonly nowadays, digital single lens reflex (DSLR)) equipped with a specialized hemispherical lens and self-levelling tripod. For the most accurate estimates, images must be acquired against uniformly overcast skies or the fleeting light at dusk or dawn with the camera level to the horizon and with closely calibrated exposure. The reliance on DSLRs stems from the need to manually fine-tune exposure and the advantage of large sensors. Large sensors record more pixels per area of view and more information per pixel, which translates to more accurate classification of canopy elements. Careful tuning of exposure settings is critical to avoid major inaccuracies in final estimates (Zhang *et al.* 2005; Beckschäfer *et al.* 2013).

Typical camera and hemispherical lens systems are expensive and challenging to deploy in the field. In response, researchers have attempted to develop new methods including using smartphones with clip-on lenses (Tichý 2016; Bianchi *et al.* 2017) and eschewing specialized levelling devices (Origo *et al.* 2017), to varying success. These smartphone-based methods are limited by small sensors and the low quality of aftermarket fisheye lenses. Other researchers have developed methods that use standard cameras with reduced field-of-view lenses and account for non-hemispherical images (i.e. restricted view photography) to estimate canopy structure with less sensitivity to camera exposure while maximizing the full frame of the

© The Author(s) 2021. Published by Oxford University Press on behalf of Institute of Chartered Foresters. All rights reserved. For permissions, please e-mail: journals.permissions@oup.com

Downloaded from https://academic.oup.com/forestry/advance-article/doi/10.1093/forestry/cpab034/6320703 by Yale University Law School user on 17 July 2021

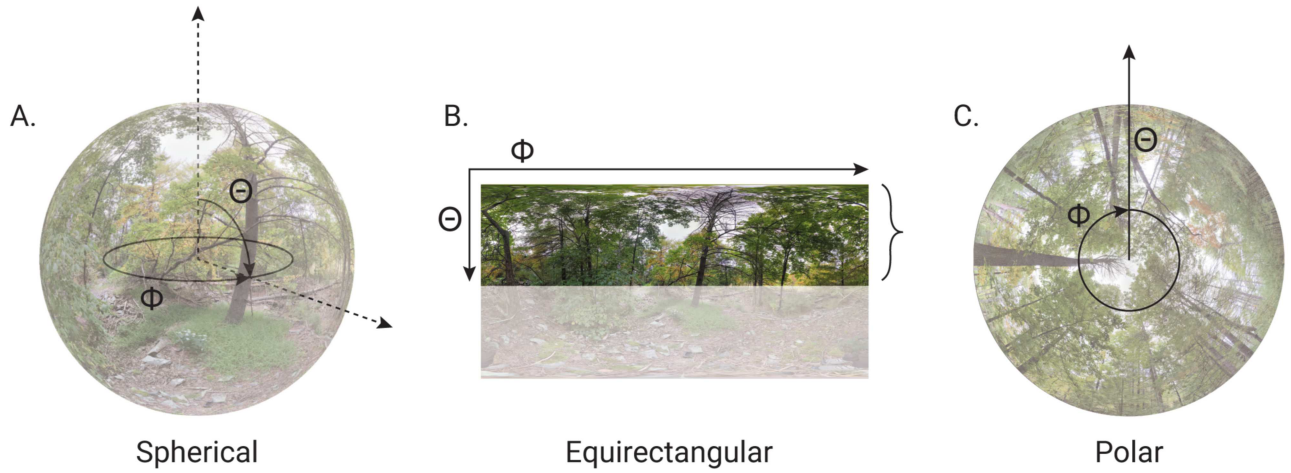

Figure 1 Spherical panoramas (A) are stored and output from smartphones as 2D images with equirectangular projection (B). Because spherical panoramas are automatically levelled using the phone gyroscope, the top half of the equirectangular image corresponds to the upper hemisphere of the spherical panorama. The top portion of the equirectangular image (B) can then be remapped onto the polar coordinate plane to create a circular hemispherical photo (C). In all images, zenith and azimuth are indicated by Θ and Φ, respectively.

sensor (Chianucci 2020). Yet, without a full hemisphere of view, this method cannot be used for estimating light environments. Thus, despite the fact that almost all ecologists and foresters carry a high-powered, image processing device in our pockets, we have yet to fully employ it for the purpose of data collection.

Here, I test a novel method of acquiring HP images from smartphone spherical panoramas (SSP HP) for estimating canopy measures. This method leverages the advantages of restricted view photography and the utility of smartphones to produce true circular HP images at higher resolution than traditional DSLR HP without the need for additional equipment (i.e. levelling device or lens). I compare estimates from HP images extracted from SSP HP to traditional DSLR HP images and an alternative smartphone method with a fisheye lens that was proposed by Bianchi *et al.* (2017).

Spherical panoramas can be generated on any modern smartphone with pre-installed software like Google Camera (Google LLC), or free applications like Google Street View (Google LLC) (available for Android OS or iOS). With Google Camera, spherical panoramas are composed from 36 individual images with limited field-of-view (57° field-of-view with Google Pixel 4a). Images are acquired by rotating the camera around a central point, guided by the camera's spatial mapping and aided by the device's internal gyroscope and compass. The smartphone camera software automatically merges the individual images into a spherical projection using interest point detection and scale invariant feature transformation to accommodate imperfect viewing distance and viewing angle between images (Szeliski and Shum 1997; Brown and Lowe 2007). Spherical panoramas are recorded in equirectangular projection from which the top half can be easily remapped into polar projection as a circular HP (Figure 1).

Modern smartphones overcome physical limitations of small optics and sensors by employing computational photography techniques that merge multiple images to create a single, high resolution image (Barbero-García *et al.* 2018). The result is a composite image that retains the sharpest elements and most even exposure of each individual photo that is sharper (Gunturk 2017) and with greater dynamic range than any individual photo (Lukac 2017). Modern computational photography with small sensors can rival images produced by much larger, DSLR-sized sensors (Ignatov *et al.* 2017).

Methods

I estimated canopy structure and light values from two sources: hemispherical photos captured with a DSLR camera (Canon 60D; Canon Inc., Tokyo, Japan) equipped with a circular hemispherical lens (Sigma 4.5 mm f2.8 EX DC; Sigma Corp., Ronkonkoma, NY, USA) and spherical panoramic images captured with a smartphone (Pixel 4a; Google LLC, Menlo Park, CA, USA) and native spherical panorama software (Google Camera v.8.1.011.342784911). In addition, I simulated images to approximate the method proposed by Bianchi *et al.* (2017) using a smartphone with clip-on fisheye lens.

I acquired images from 35 sites at Yale Nature Preserve, New Haven, CT, USA and 37 sites at Rockstock property, Woodstock, NY, USA on 4 July 2020 and 27 September 2020, respectively. Yale Nature Preserve is comprised of low-elevation rocky ridges separating wet valleys and vernal wetlands. The canopy is composed of mixed hardwoods, predominantly *Acer rubrum*, *Quercus rubra*, *Fagus grandifolia*, *Carya tomentosa*, *Quercus bicolor* and *Liriodendron tulipifera*. Rockstock property is an historical Northeastern farmstead and wetland on which a mixed forest of northern hardwoods (*Acer saccharum*, *Carya ovata*, *Quercus rubra*, *Acer pensylvanicum* and *Betula lenta*) and conifers (*Pinus strobus* and *Tsuga candensis*) have recolonized since the early twentieth century.

Photo sites were selected to represent a distribution of canopy species (deciduous, coniferous and mixed), openness and gap

Downloaded from https://academic.oup.com/forestry/advance-article/doi/10.1093/forestry/cpab034/6320703 by Yale University Law School user on 17 July 2021

size. All images were captured at breast height (approximately 1.3 m) on uniformly overcast days with smartphone images taken immediately following each DSLR image.

DSLR protocol

Prior to image acquisition, I established exposure settings two stops overexposed relative to open sky following Brown *et al.* (2000) and Beckschäfer *et al.* (2013) with maximum ISO values of 1000 and minimum shutter speed of 1/100 s (Chianucci and Cutini 2012). Images were recorded in Canon RAW format (.CR2) with the camera oriented perpendicular to gravity enabled by a dual-axis gimbal and with the top of the image oriented towards magnetic north.

Even on uniformly overcast days, the sky brightness changes over time. To account for this, I adjusted white point values in Adobe Lightroom 5.7.1 to ensure that the grey value of the brightest sky pixels aligned to full white (Beckschäfer *et al.* 2013) and exported the images as full-resolution (5184 × 3456 pixels) JPEG files. These images are considered the standard reference for comparison throughout further analysis.

To compare the discrepancy due to image acquisition methods to the discrepancy due to incorrect exposure, I additionally created output files with exposure values adjusted 1, 2, 3, 4, or 5 values above and below the original exposure in Adobe Lightroom. I included a circular mask along the perimeter of the circular image to prevent glare at the margins from impacting downstream estimates.

SSP *protocol*

I created spherical panoramas using a Pixel 4a smartphone—Google's mid-range consumer-grade smartphone model—with the Google Camera application. Spherical panoramas are composed from 36 overlapping images of the entire 360° field-of-view. I began each spherical image sequence facing towards magnetic north (azimuth 0°; this becomes the top of the circular hemispherical image after processing). For this study, I ascertained a northern heading with an external compass first for DSLR HP and used this to orient the SSP HP. However, the yaw angle from the metadata of the resulting SSP HP image can be used to rotate the image to the proper orientation in post-processing regardless of the direction of capture (Li and Ratti 2019). The first image of the panorama must be taken with the phone levelled to the horizon; the camera software facilitates this by placing a dot on the screen and disallowing images with too great of pitch or roll to the camera. Subsequent images are similarly guided by on-screen targets. Twelve images centred along the horizon comprise zenith 72°–108°. Nine images in the upper and lower hemisphere cover zenith 36°–72° or 108°–144°, respectively. Similarly, three images each comprise the remaining area at the poles. Although no order is specified by the application, I followed the same capture order for every spherical panorama, first rotating to capture the 12 images sequentially around the horizon. Next, I sequentially captured the nine images for zenith 36°–72°, followed by three images for zenith 0°–36°. I then followed the same order in the lower sphere. The phone's internal gyroscope is used to automatically level the horizon of the sphere. Care must be taken to rotate and pan the smartphone camera treating the camera as the centerpoint, rather than rotating the camera around one's body.

Spherical panoramas are created by tiling multiple planar images into a geodesic polyhedron and then stitching the images into a spherical, omnidirectional image which can be viewed in 3D (Fangi and Nardinocchi 2013). The spherical images are mapped into two dimensions following an equirectangular projection in which the zenith angle corresponds to the rectangular *y*-axis and azimuth angle corresponds to the rectangular *x*-axis (Fangi and Nardinocchi 2013) (Figure 1). Conveniently, when the sphere is levelled to the horizon, the top half of the rectangular panoramic image depicts the upper hemisphere of view and can be cropped and remapped into a polar projection (e.g. Li and Ratti 2019).

I extracted the top half of the equirectangular panorama JPEG file (i.e. the top hemisphere) and converted it to a circular hemispherical image via polar projection in GIMP (Gnu Image Manipulation Program v.2.10.20) with batch processing implemented in BIMP (Batch Image Manipulation Plugin v.2.4) (setting files are included in the data archive along with scripts for an alternative processing from the command line with ImageMagick v.7.0.10).

Transformation from equirectangular to polar projection with square pixels requires either downsampling pixels closer to the pole or interpolating pixels near the horizon, or both. I retained the width of the equirectangular image in the transformation to polar projection, resulting in a SSP HP image with diameter equal to the width of the equirectangular projection. Thus, the circumference of the HP at zenith 57° (∼1 radian), is equal to the width of the equirectangular image. Pixels circumscribing zenith angles greater or less than 57° are upscaled or downsampled, respectively. The result is a true HP with over 900 per cent of the resolution of traditional DSLR HP images. Because the area of the SSP HP image is larger than the upper half of the equirectangular image (i.e. more upscaling than downscaling), I test the impact of resolution below.

Unlike DSLR images, the white point does not need to be adjusted for smartphone images as this is automatically controlled by the device's high dynamic range (HDR) routine. However, the HDR routine yields a more homogenous histogram and consolidates pixel values at the mid-tones (Figure 2), which can make it difficult for binarization algorithms to differentiate between sky and canopy pixels. Contrast-stretching can facilitate pixel classification (Macfarlane *et al.* 2014). To test the effect of contrast-stretching, I output two sets of SSP HP images with and without expanding the tonal range by 5 (2 per cent) in GIMP prior to polar projection conversion.

Circular hemispherical images from DSLR photos (diameter: 2885 p; area: 6.5 MP) are considerably smaller than those produced from photo spheres (diameter: 8704 p; area: 59.5 MP). Resolution can impact canopy estimate because larger portions of the hemisphere are averaged into each pixel, leading to higher proportion of mixed pixels and underestimates of small gaps (Macfarlane 2011). To test the impacts of the resolution gain of the SSP HP, I exported an additional set of images downsampled to match the diameter of the DSLR photos (2885 p) in GIMP.

Downloaded from https://academic.oup.com/forestry/advance-article/doi/10.1093/forestry/cpab034/6320703 by Yale University Law School user on 17 July 2021

Fisheye lens simulation

Bianchi *et al.* (2017) proposed a method of approximating hemispherical photos from two perpendicular smartphone images using a fisheye lens adapter with 150° diagonal field-of-view. In order to compare this technique to the SSP HP method proposed in this study, I used the SSP HP images to simulate images from two perpendicular Pixel 4a photos captured with such a lens. I downsampled the SSP HP images to 6049 p diameter and applied a black mask that simulates Pixel 4a image dimensions (5802 × 4352 p) with 150° field-of-view.

Analysis

Binarization and canopy estimates

The processing steps above yielded 16 sets of HP images in JPEG format for each of the 72 sites (Figure S1): standard DSLR HP images (no exposure adjustment), 10 sets of exposure-adjusted DSLR HP images, four sets of SSP HP images at full or low resolution with or without contrast adjustment, and one set of fisheye HP images with appropriate contrast adjustments (Figure S2). From this point, all images received the same processing steps.

I binarized images with the Hemispherical 2.0 plugin (Beckschäfer 2015) for ImageJ v.1.51 k which uses the 'Minimum' algorithm (Prewitt and Mendelsohn 1966), which was found to produce the most accurate threshold for HP images (Glatthorn and Beckschäfer 2014). This algorithm is applied to the blue colour channel of the image to automatically classify pixels and output binary images in TIFF format (Beckschäfer 2015). During binarization, the program estimates total gap area and number of gaps, which I recorded for further analysis. I converted the binary TIFF files to BMP format in batch with ImageJ.

I used Gap Light Analyzer v.2.0 (Frazer *et al.* 1999) to estimate additional canopy structure measures and light transmittance, including CO, LAI and global site factor (GSF) measures, for further analysis. I used identical configuration parameters for all image sets with two exceptions. One, I adjusted the lens projection parameters per camera device. Two, I adjusted coordinates, elevation and declination per location. HP images created from spherical panoramas conform to true polar projection whereas the Sigma hemispherical lens used for DSLR HP images conforms to an equisolid projection (see parameter and lens configuration files in data archive). Gap Light Analyzer is implemented in a graphical interface without an option for command line input. So, I wrote a custom macro-script in AutoHotKey v.1.1.33.02 to batch process the images (script available in the data archive).

Statistical analysis

All statistical analyses were performed in R v.3.6.2 (R Core Team 2019). I used ordinary least squares and mixed effect regression models to compare differences between multiple image sets. I focused on three HP image characteristics—number of gaps, total gap area and relative gap size—to evaluate the difference in image quality between methods. I focused on three canopy measures—CO, effective LAI and GSF—to evaluate the similarity of canopy estimates between methods. Gap fraction, the ratio of white to total pixels, is the most foundational measure of HP. CO is similar to gap fraction, but weights pixels by zenith angle and is a more appropriate measure when comparing HP images with different lens distortion that biases gap size at different zenith angles (Frazer *et al.* 1997; Gonsamo *et al.* 2013). I calculated relative gap size as the area of the mean canopy gap, standardized to the total image size which is equal to CO divided by the number of gaps. LAI is a comparison of leaf area relative to horizontal ground area, formally defined as the ratio of single-side leaf area to a given area of horizontal ground footprint (Chen and Black 1992). In Gap Light Analyzer, LAI is integrated over zenith angles 0°–60° following Stenberg *et al.* (1994). Because no distinction is made between foliage and stem canopy elements nor between broad-leaves and needles in the calculation, LAI estimated in Gap Light Analyzer is effectively a plant area index. GSF is a measure of through-canopy radiation. It is the weighted average of the proportion of direct and indirect radiation transmitted through the canopy to that above the canopy (Anderson 1964). The three canopy measures are a function of the image quality measures and represent the range of the inference for which researchers use HP.

Indirect estimates of LAI from HP rely on the commonly violated assumption that leaves are randomly distributed in the canopy (Yan *et al.* 2019). To overcome this limitation, analytical methods have been developed to estimate and correct for the clumping effect in canopies by systematically excluding large between-crown gaps from small within-crown gaps to calculate a clumping index (e.g. Chen and Cihlar 1995). However, the poor resolution of traditional DSLR HP makes gap classification ineffective at low zenith angles and in dense canopies (Yan *et al.* 2019; Chianucci 2020). The high resolution of SSP HP is likely overcome such limitations and produce more accurate calculations of clumping. To illustrate the differences, I additionally compare clumping index estimates from full-resolution SSP HP and DSLR HP, using the gap thresholding method established by Alvernini *et al.* (2018) (see Supplemental Materials for details).

I tested for differences in canopy structure and light environment measures across all image processing methods by fitting linear mixed effect models with the unique image site as a random intercept (i.e. a repeated measures analysis). I regressed each canopy and image quality measure against the image acquisition and processing protocol as the independent variable with the standard DSLR HP image as the reference. I fit mixed effect models in 'lme4' (Bates *et al.* 2015) and estimated parameters and 95 per cent confidence intervals with 1000 nonparametric bootstrap iterations. Additionally, I fit bivariate ordinary least squares models regressing canopy measures estimated from each image processing protocol on the standard DSLR HP estimates. For these models, the effect size of the dissimilarity between image sets is measured by the magnitude of the deviation of the slope from 1 or the intercept from 0 and the coefficient of determination indicates the appropriateness of the image processing protocol as an alternative to traditional DSLR HP. In all model sets, the variability among estimates from under- or overexposed DSLR HP can be used as a qualitative gauge of the effect size between SSP HP methods.

Downloaded from https://academic.oup.com/forestry/advance-article/doi/10.1093/forestry/cpab034/6320703 by Yale University Law School user on 17 July 2021

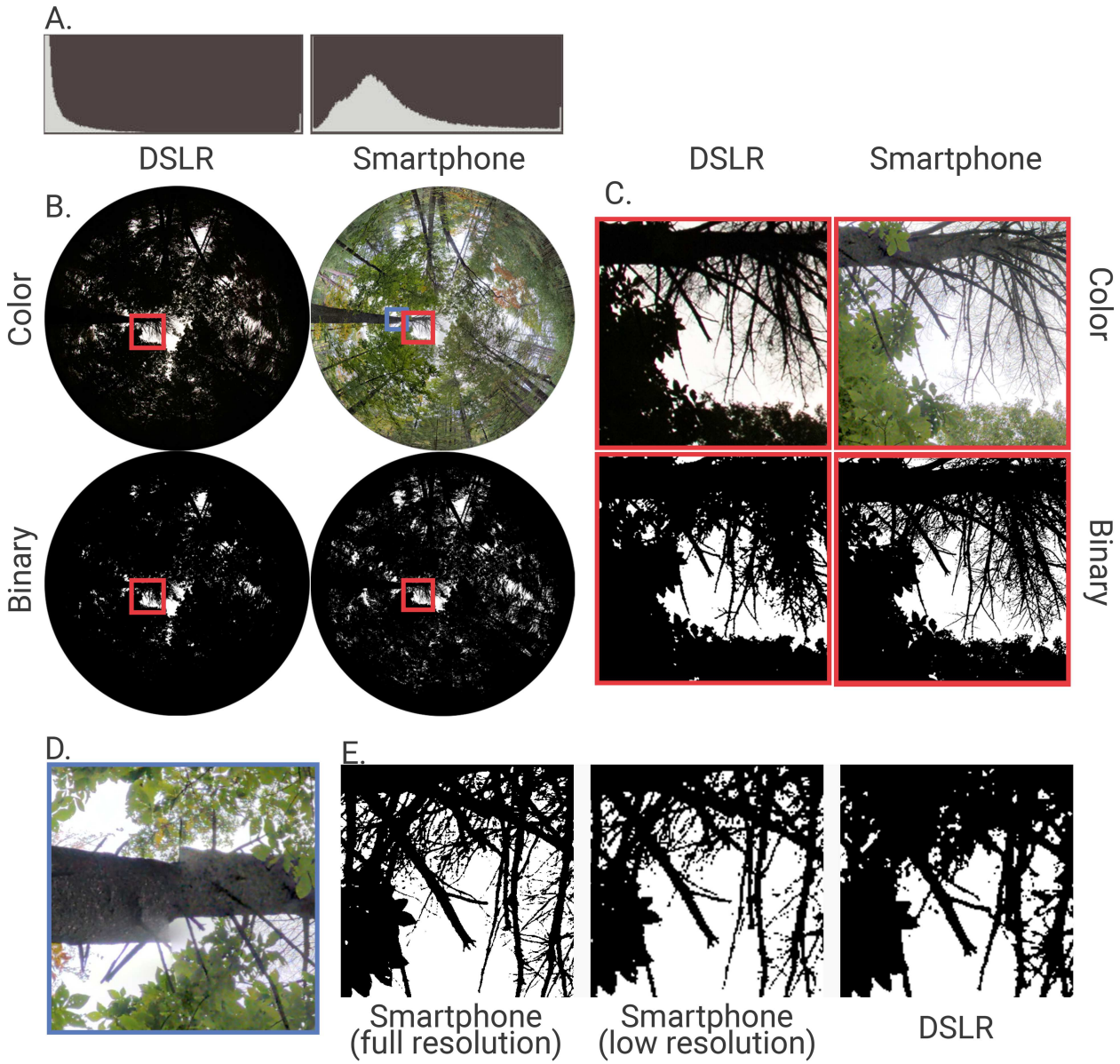

Figure 2 Comparisons of images generated with smartphone spherical panorama hemispherical photography (SSP HP) (right B and C) to traditional DSLR hemispherical photography (DSLR HP) (left B and C) captured at the same site. Details of a subsection of the canopy, indicated by orange boxes, are expanded in C. Binarized images are shown below colour images in B and C. Image histograms differ in the distribution of luminance values in the blue colour plane (A). In panel E, a section of the canopy from a binary full-resolution SSP HP image (left), downsampled SSP HP image (middle), and DSLR HP image (right) is further expanded to demonstrate the effect of image clarity on pixel classification. An example of an incongruous artefact resulting from misalignment in the spherical panorama is outlined in blue in B and expanded in D. SSP HP images were generated from spherical panoramas taken with Google Pixel 4a and Google Camera. DSLR HP images were captured with Canon 60D and Sigma 4.5 mm f2.8 EX DC hemispherical lens.

Results

The canopies surveyed in this study ranged from densely closed ($CO_{min} = 1$ per cent, $GSF_{min} = 1$) to moderately open ($CO_{max} = 40$ per cent, $GSF_{max} = 63$). Most sites skew towards denser canopies ($CO_{IQR} = 2$ per cent–6 per cent, $GSF_{IQR} = 3$–9). This is advantageous for the purpose of this study as estimates from dense canopies are substantially more sensitive to HP settings (Beckschäfer *et al.* 2013). There was no significant difference between locations (all $P > 0.08$; Table S1).

HP images generated from spherical panoramas were noticeably sharper than those captured with a DSLR and hemispherical lens (Figure 2C and E). The greater sharpness resulted in more definition of fine canopy structure even when scaled to the same resolution (Figure 2E). Close inspection of the smartphone HP reveals occasional infidelities arising from the process of stitching

Downloaded from https://academic.oup.com/forestry/advance-article/doi/10.1093/forestry/cpab034/6320703 by Yale University Law School user on 17 July 2021

the panoramas (Figure 2D). These artefacts appear as discontinuities or overlapping of canopy elements.

Effect of contrast-stretching on SSP HP

Unlike most DSLR HP images, which exhibit bimodal distribution of pixel tones, the HDR pre-processing of smartphone cameras produces images with tonal values with a normal distribution centred around the midpoint tone (Figure 2A). This poses a problem for binarization algorithms that iteratively seek a global minimum along the histogram and can lead to extreme overclassification of sky pixels at lower resolutions or restricted field-of-view. One full-resolution SSP HP image (1 per cent) and three low resolution SSP HP images (4 per cent) were incorrectly classified and easily identified as outliers (Figure S3). Twelve fisheye HP images (17 per cent) were incorrectly classified. I applied a 2 per cent contrast-stretch to all SSP HP images and up to 8 per cent as needed for fisheye HP images to ensure no misclassifications.

Without contrast adjustment, CO and GSF from full-resolution SSP HP images are overestimate by 18 per cent and 12 per cent whereas LAI is underestimated by less than −1 per cent relative to the corrected image set (Table 1). The effect of contrast-stretching is much stronger for estimates from low resolution images due to the greater number of incorrectly binarized outlier images. Relative to corrected images, CO and GSF are overestimated by 56 per cent and 37 per cent, respectively and LAI is underestimated by −2 per cent when low resolution SSP HP are not corrected with contrast-stretching (Table 1). Only the contrast adjusted images were retained for further analysis.

Effect of resolution on SSP HP

Downsampling SSP HP images from 59.5 MP to 6.5 MP (−815 per cent) to match the resolution of DSLR HP images resulted in nearly half the number of gaps (−48 per cent) of larger relative size (+142 per cent) compared to the full-resolution SSP HP image set (Table 1). Downsampling had minimal effect on canopy structure and light estimates, however (Table 1, Figure 3). Downsampling resulted in only a 1 per cent decrease in CO and 2 per cent decrease in GSF in relation to the standard reference compared to full-resolution SSP HP images (Table 1). Downsampling had a similarly minimal effect of increased LAI (1 per cent) (Table 1). Reduction in resolution increased variance in CO (1 per cent), GSF (1 per cent) and LAI (4 per cent) for the entire image set, but decreased the variance in number of gaps (−61 per cent) and gap area (−89 per cent) considerably (Table 2, Figure 4). Downsampled images exhibited greater variance in relative gap size (+107 per cent) (Table 2).

Comparison to DSLR HP

Full-resolution SSP HP images retained more gaps (493 per cent) and smaller relative gap size (−79 per cent) compared to DSLR HP (Table 1, Figure 4). Although downsampling reduces the difference, SSP HP images with the same resolution as DSLR HP images exhibit more (209 per cent) gaps of smaller relative size (−49 per cent) (Table 1). The difference in relative gap size increases with greater CO (Figure 5). Despite the larger difference in gap number, the total gap area in downsampled smartphone images was just 19 per cent larger than DSLR HP reference images on average (Table 1).

Estimates from SSP HP images were greater for CO (Full = +23 per cent, Low = +22 per cent), greater for GSF (Full = +18 per cent, Low = 16 per cent) and lower for LAI (Full = −19 per cent, Low = −18 per cent) compared to the reference DSLR HP images (Table 1, Figure 4). All canopy measures based on SSP HP images tend to overestimate the reference DSLR HP images at low values but underestimate at higher values (Figure 3). In general, these differences are comparable to the effects of overexposing DSLR images by 1–1.5 stops (Figures 4 and S4). SSP HP estimates of CO and GSF were highly correlated with DSLR HP estimates ($R^2 > 0.9$) whereas LAI was moderately correlated ($R^2 = 0.71$) (Table S2, Figure S5).

Comparison to 150° field-of-view fisheye HP

HP images emulating perpendicular 150° field-of-view fisheye images were moderately to highly correlated with the reference DSLR HP images for CO ($R^2 = 0.87$), GSF ($R^2 = 0.89$) and LAI ($R^2 = 0.66$) but less so than true HP produced by spherical panoramas (Figure S5, Table S2). Fisheye HP image values tended to result in overestimates of CO (+6 per cent) and GSF (+7 per cent), relative to full-resolution SSP HP images, on average (Table 1). The restricted field-of-view of the fisheye images tend to underestimate LAI more so than full-resolution SSP HP (−7 per cent) (Table 1). Estimates from the fisheye HP method are comparable to DSLR HP images 1–2 stops overexposed (Figures 4 and S4).

Comparison of clumping index

SSP HP recovers more gaps in total (Table 1), but also tends to recover a higher proportion (+ 64 per cent) of between-canopy gaps (i.e. large gap fraction) relative to DSLR HP (Figure S6). Correspondingly, crown porosity tends to be greater (61 per cent) when estimated from SSP HP (Figure S6). As a result, DSLR HP tends to overestimate clumping (2 per cent), especially in denser canopies (3.4 per cent overestimation in canopies under 10 per cent openness) (Figure S6).

Discussion

Smartphones have become nearly ubiquitous, yet researchers typically do not exploit even a fraction of their potential as a research tool. HP generated from SSP offers a highly accurate alternative to traditional DSLR HP with over 90 per cent correlation with traditional methods for common canopy and light measures. The difference between estimates of canopy structure and light environment from spherical panoramas vary from the reference photos by about the same as over- or underexposing images by 1–1.5 stops.

The primary differences between SSP HP and DSLR HP are that the former produces larger images, sharper resolution and more even tonal range across the image. SSP HP images generated with the Google Pixel 4a smartphone are over nine times larger than those taken with a DSLR. However, the simple increase in resolution does not account for the difference in clarity, as downsampled SSP HP images still retain more fine structure than DSLR

Downloaded from https://academic.oup.com/forestry/advance-article/doi/10.1093/forestry/cpab034/6320703 by Yale University Law School user on 17 July 2021

Table 1 Linear mixed effect model coefficients and 95 per cent confidence intervals for three canopy measures and three image quality metrics estimated from images acquired with traditional DSLR camera and hemispherical lens or extracted from smartphone spherical panoramas (SSP) and processed with difference protocols. For all models, the unique site of image acquisition was estimated as a random intercept ($N_{obs} = 1152$, $N_{sites} = 72$). Coefficients that significantly differ from the $DSLR_{standard}$ reference images (i.e. 95 per cent confidence interval does not include 0) are indicated in bold. Coefficients and confidence intervals were estimated with 1000 non-parametric bootstraps.

Image set	Canopy openness (%)	Leaf area index	Global site factor	Gap Area (MP)	Number of gaps ($\times 10^3$)	Relative gap size ($\times 10^{-3}$)
$DSLR_{Standard}$ (Intercept)	**5.49** (**3.45**, **7.65**)	**4.19** (**3.66**, **4.69**)	**8.23** (**5.68**, **11.05**)	0.37 (−0.09, 0.88)	**4.14** (**3.50**, **4.80**)	1.23 (−7.19, 9.04)
SSP_{Full}	1.29 (−1.15, 3.64)	**−0.78** (**−1.39**, **−0.16**)	1.47 (−0.88, 3.69)	**3.66** (**2.98**, **4.27**)	**20.41** (**19.62**, **21.22**)	−0.97 (−12.61, 10.39)
SSP_{Low}	1.20 (−1.15, 3.32)	**−0.74** (**−1.36**, **−0.15**)	1.32 (−0.97, 3.58)	0.07 (−0.56, 0.67)	**8.67** (**7.92**, **9.45**)	−0.60 (−11.11, 11.13)
$SSP_{Full\ (uncorrected)}$	2.48 (0.12, 4.89)	**−0.80** (**−1.37**, **−0.21**)	**2.59** (**0.32**, **4.83**)	**4.36** (**3.75**, **4.97**)	**20.08** (**19.21**, **20.96**)	0.12 (−10.34, 11.24)
$SSP_{Low\ (uncorrected)}$	**4.95** (**2.66**, **7.30**)	**−0.83** (**−1.44**, **−0.20**)	**4.88** (**2.62**, **7.25**)	0.30 (−0.35, 0.92)	**7.81** (**7.02**, **8.62**)	**23.49** (**12.94**, **33.95**)
$SSP_{Fisheye}$	1.72 (−0.40, 4.10)	**−1.01** (**−1.61**, **−0.45**)	2.15 (−0.11, 4.44)	**1.58** (**0.94**, **2.22**)	**14.93** (**14.18**, **15.73**)	−0.78 (−12.55, 10.50)
$DSLR_{Exp-5}$	**−3.93** (**−6.24**, **−1.72**)	**7.09** (**6.51**, **7.72**)	**−5.92** (**−8.30**, **−3.60**)	−0.26 (−0.92, 0.35)	**−3.42** (**−4.26**, **−2.61**)	−0.31 (−11.73, 10.86)
$DSLR_{Exp-4}$	**−3.20** (**−5.25**, **−0.91**)	**4.40** (**3.76**, **5.02**)	**−4.90** (**−7.26**, **−2.51**)	−0.23 (−0.80, 0.44)	**−2.81** (**−3.61**, **−2.04**)	0.15 (−9.77, 11.60)
$DSLR_{Exp-3}$	−1.67 (−3.96, 0.54)	**2.60** (**2.01**, **3.22**)	**−2.50** (**−4.75**, **−0.25**)	−0.10 (−0.72, 0.46)	**−2.03** (**−2.91**, **−1.25**)	0.47 (−10.81, 11.43)
$DSLR_{Exp-2}$	−1.39 (−3.67, 0.92)	**1.26** (**0.66**, **1.87**)	−1.93 (−4.15, 0.19)	−0.10 (−0.74, 0.54)	**−1.73** (**−2.51**, **−0.92**)	0.33 (−10.56, 11.69)
$DSLR_{Exp-1}$	−0.78 (−3.13, 1.63)	0.56 (−0.05, 1.15)	−1.14 (−3.42, 1.18)	−0.04 (−0.69, 0.61)	**−0.95** (**−1.81**, **−0.17**)	0.44 (−10.90, 11.40)
$DSLR_{Exp+1}$	1.36 (−0.86, 3.51)	−0.58 (−1.18, 0.04)	1.92 (−0.37, 4.11)	0.09 (−0.54, 0.74)	**1.48** (**0.71**, **2.27**)	−0.02 (−11.40, 12.75)
$DSLR_{Exp+2}$	**3.22** (**1.13**, **5.63**)	**−1.07** (**−1.71**, **−0.49**)	**4.59** (**2.17**, **6.98**)	0.22 (−0.38, 0.87)	**3.07** (**2.30**, **3.88**)	0.00 (−11.07, 11.65)
$DSLR_{Exp+3}$	**6.04** (**3.65**, **8.32**)	**−1.59** (**−2.20**, **−0.96**)	**8.38** (**6.11**, **10.73**)	0.44 (−0.22, 1.08)	**4.58** (**3.81**, **5.41**)	0.31 (−10.31, 11.84)
$DSLR_{Exp+4}$	**9.94** (**7.66**, **12.10**)	**−2.00** (**−2.58**, **−1.38**)	**13.54** (**11.32**, **15.86**)	**0.68** (**0.06**, **1.29**)	**5.80** (**5.00**, **6.57**)	0.63 (−11.06, 11.77)
$DSLR_{Exp+5}$	**15.87** (**13.54**, **18.08**)	**−2.38** (**−2.99**, **−1.79**)	**20.53** (**18.23**, **22.90**)	**1.10** (**0.49**, **1.73**)	**7.41** (**6.59**, **8.21**)	1.37 (−9.42, 12.69)

Table 2 Comparison of canopy measures and image quality metrics estimated from full-resolution smartphone spherical panorama hemispherical photography imagesets and the same imageset downsampled to the same area as DSLR hemispherical photography images.

Measure	Full Resolution Mean (SD)	Low Resolution Mean (SD)	% Difference of Mean	% Difference of SD
Canopy openness (%)	6.78 (5.35)	6.7 (5.41)	-1.15	0.96
Global site factor	9.69 (8.95)	9.56 (8.99)	-1.31	0.48
Leaf area index	3.19 (0.59)	3.23 (0.62)	1.01	4.25
Gap area (MP)	4.02 (3.18)	0.44 (0.36)	-89.16	-88.95
No. of gaps ($x10^3$)	24.53 (5.08)	12.82 (19.82)	-4.78	-6.10
Relative gap size ($\times 10^{-3}$)	0.29 (0.27)	0.55 (0.55)	91.01	106.89

Downloaded from https://academic.oup.com/forestry/advance-article/doi/10.1093/forestry/cpab034/6320703 by Yale University Law School user on 17 July 2021

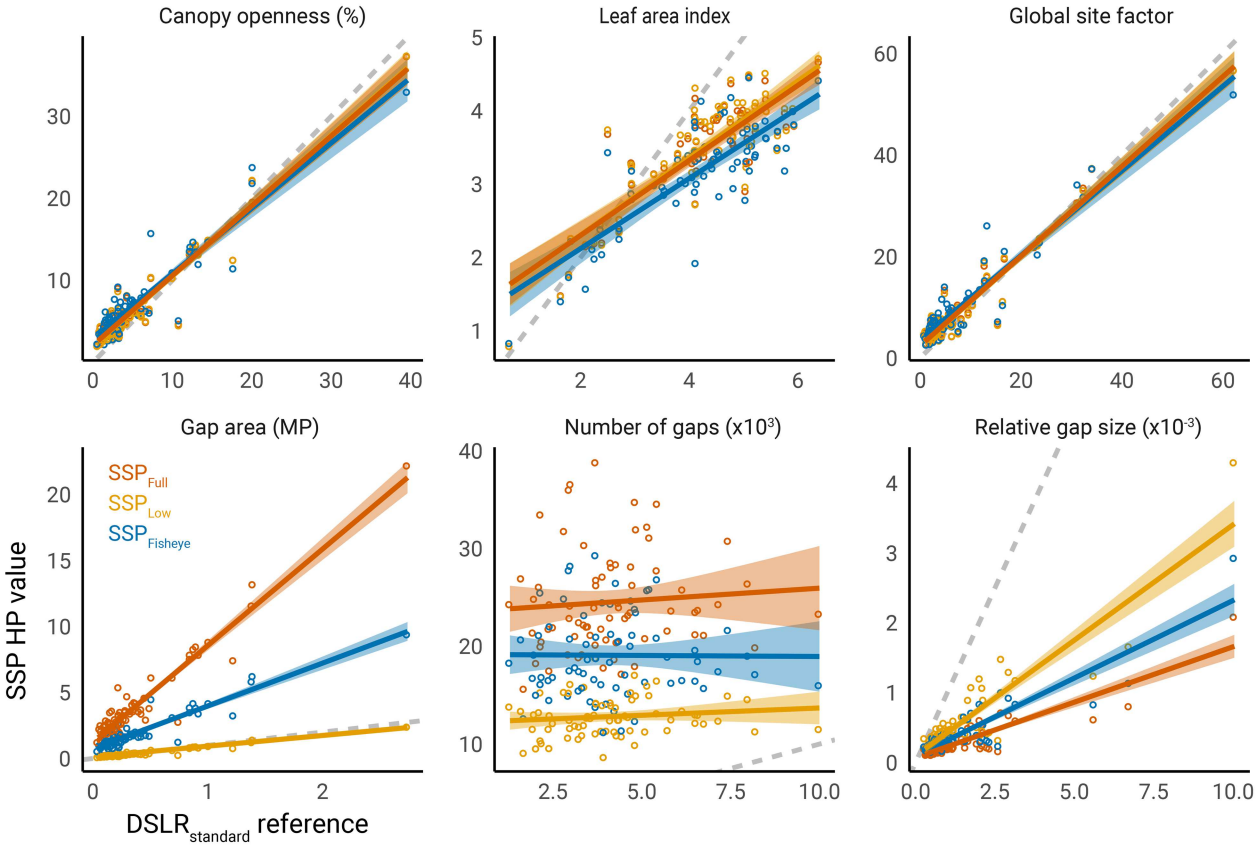

Figure 3 Linear regression estimates comparing three canopy structure measures (canopy openness, leaf-area index (LAI), and global site factor (GSF)) and three image quality metrics (total gap area, number of gaps, and relative gap size) from hemispherical images extracted from smartphone spherical panoramas (SSP) to those acquired with traditional DSLR camera and hemispherical lens ($DSLR_{Standard}$). Three processing methods for SSP hemispherical images were compared, including full resolution (SSP_{Full}, dark orange), images downsampled to match the resolution of DSLR images (SSP_{Low}, light orange), and images simulated to approximate Bianchi *et al.* (2017) method using a smartphone and clip-on fisheye lens ($SSP_{Fisheye}$, blue) are shown. The 1:1 line is indicated by a dashed grey line. Figure S4 additionally shows the comparison of exposure setting for DSLR images.

HP images of the same size. When comparing DSLR HP images to those from SSP HP at the same resolution, it is clear that DSLR HP tends to result in underestimation of the number of canopy gaps. This is due to low clarity causing adjacent pixels to bleed into each other, even when generated with industry standard lens and camera. Thus, the smallest gaps tend to be lost and small gaps tend to collapse into larger gaps more quickly, as evidenced by higher relative gap size across all canopy densities. This second point can be seen in the way relative gap size increases with CO much faster for DSLR HP. Thus, although SSP HP images contain many more total gaps, the total gap area is similar, albeit with slightly more relative gap area as a consequence of retaining small gaps. The retention of small gaps in SSP HP offers great potential in using crown clumping indices to correct LAI estimates for non-randomly distributed canopy elements.

The difference in clarity is most likely a product of the restricted field-of-view of individual photos included in the panorama, improved sharpening through computational photography, and homogenous tone across zenith regions. In contrast, DSLR HP images suffer from glare and hazing associated with extremely wide field-of-view lenses. In addition, DSLR cameras struggle to evenly expose the entire hemisphere in a single exposure. For these reasons, SSP HP is likely to be far more robust to non-optimal lighting conditions, but more studies in variable skies are needed. An additional advantage of SSP HP is that, unlike DSLR methods, automatic exposure aided by HDR effectively obviates the need for tedious manual exposure settings. Although this can introduce errors in binarization, minimal contrast-stretching solves the issue. Improvements in pixel classification beyond simple thresholding (e.g. Díaz *et al.* 2021) are likely to make this a non-issue even in direct sunlight conditions.

Although many canopy and light estimation software programs require hemispherical images, panoramic images could be directly processed without re-projecting them into polar coordinates if estimates of light environment are not needed (e.g. Grotti *et al.* 2020). Directly processing panoramic projections has the advantage of retaining more pixels closer to the zenith which may improve accuracy of estimating gap fraction, especially in denser canopies (Chianucci *et al.* 2019). Retaining panoramic projections would additionally allow for direct comparison and validation

Downloaded from https://academic.oup.com/forestry/advance-article/doi/10.1093/forestry/cpab034/6320703 by Yale University Law School user on 17 July 2021

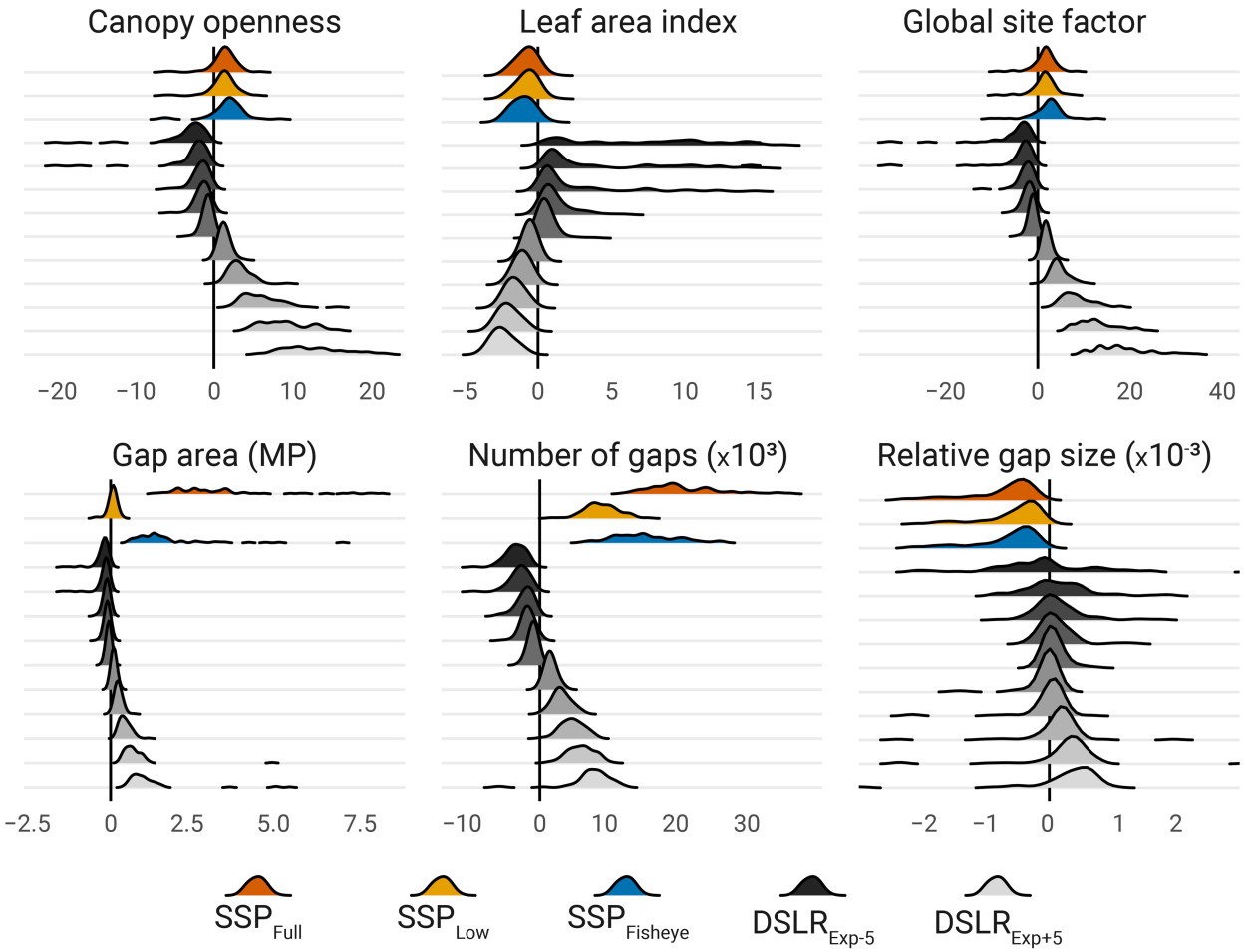

Figure 4 Difference in canopy structure and light environment estimates between reference (standard DSLR hemispherical photography (HP) images) and full-resolution smartphone spherical panorama hemispherical photography (SSP HP) images (SSP_{Full}, dark orange), low resolution SSP HP images (SSP_{Low}, light orange) downsampled to match the standard DSLR resolution, fisheye HP ($SSP_{Fisheye}$, blue), and DSLR HP images with exposure adjusted from +5 to −5 ($DSLR_{Exp}$, light to dark).

with other methods, such as terrestrial scanning lidar (Grotti *et al.* 2020).

Artefacts generated by the panorama stitching process did not have a noticeable effect on canopy and light estimates but are a potential source of error. Care during image capture can reduce most cases of incongruity, however. Spherical panorama software assumes that all images are captured by rotating the camera around a single point in space (Fangi and Nardinocchi 2013). When taking images by hand, it is easy to shift the phone, and therefore the image plane, during rotation. Practice in steady positioning helps. Also, the ability to immediately review panoramas on one's screen phone or with stereoptic headsets lets researchers catch errors and retake panoramic images in the field. This problem will attenuate as smartphone stitching software continues to improve (Luhmann 2004).

SSP HP offers practical benefits over other methods in requiring no additional equipment other than a smartphone. Levelling is achieved automatically via the phone's gyroscope. Geographic coordinates, elevation and orientation are retained in the image metadata and could easily be integrated into an analysis pipeline. Furthermore, dedicated smartphone apps could be developed to make data acquisition accessible to non-experts. The fact that waterproof housings are cheap and readily available for smartphones is another benefit to field work not to be overlooked. Coupled with the fact that SSP HP requires no tedious exposure settings and can be easily georeferenced, this method is highly amenable to citizen science projects or widespread ground-truthing of remote sensing data.

Although there is likely to be variation between smartphone models which must be validated in future studies, the lack of lenses with idiosyncratic projections removes a major source of variability. All SSP HP images have polar projection by virtue of originating as spherical images.

The method presented here outperforms other methods of capturing HP with smartphones via clip-on fisheye lenses. Simulating Bianchi *et al.* (2017) method showed that the loss of information from restricting images to 150° field-of-view results in skewed but still relatively accurate estimates of canopy structure

Downloaded from https://academic.oup.com/forestry/advance-article/doi/10.1093/forestry/cpab034/6320703 by Yale University Law School user on 17 July 2021

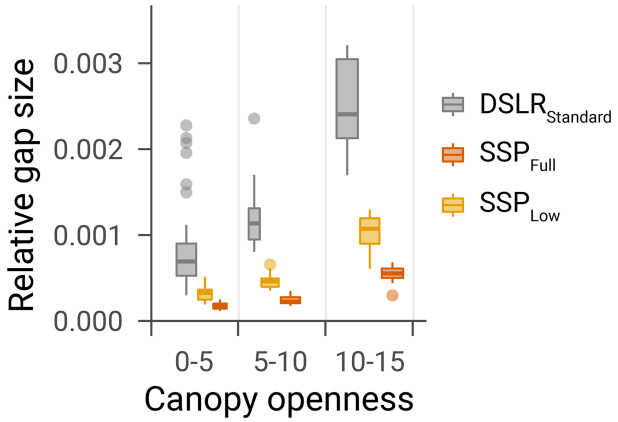

Figure 5 Relative gap size related to canopy openness for standard DSLR hemispherical photography (grey), downsampled smartphone spherical panorama hemispherical photography (SSP HP) images (SSP_{Low}, light orange), and full-resolution SSP HP images (SSP_{Full}, dark orange). Values were binned into three canopy openness thresholds (0–5, 5–10, 10–15). Canopy openness values greater than 15 per cent were excluded due to lack of sites with high values.

and light environment. However, the comparison is generous in that the fisheye HP images in this study were simulated from SSP HP images and therefore suffered no effects of poor optical quality associated with the small size of clip-on smartphone lenses.

Only the upper hemisphere was extracted from the spherical panoramas in this study, but other portions of the panorama could be extracted for other purposes. For instance, horizontal panorama could be used for estimating basal area (Fastie 2010) or mapping stands (Lu *et al*. 2019). The lower hemisphere could be useful in monitoring understory plants or ground cover composition. Researchers can even enter the spherical image with a virtual reality headset to identify species after leaving the field.

Conclusion

High-quality hemispherical images can be acquired with modern smartphones via the following protocol:

- Capture photospheres following on-screen instructions of smartphone panorama application, being careful to rotate in place with the camera lens as the centre of the sphere.
- Convert spherical panoramas to circular hemispherical images with provided scripts, or by manually extracting the upper half of the 2D Cartesian panorama, applying 2 per cent contrast-stretching, and projecting into polar coordinates.

SSP HP solves many of the problems associated with traditional HP while offering many practical benefits for field applications. The ubiquity of smartphones and their ever-improving quality of software and optical hardware will only widen the range of spherical panoramic imagery applications in silviculture and forest ecology into the future.

Supplementary materials

The following supplementary material is available at Forestry online: additional data summary tables, additional figures, and additional analyses. R code used to conduct statistical analysis and generate figures, AutoHotKey macro scripts to automate Gap Light Analyzer software, and code to batch process spherical panoramas via BIMP recipies for GIMP or via ImageMagick are available in the data repository. Additional method tutorials are available at the author's website: azandisresearch.com.

Data availability

Code for analysis and image processing is available at: github.com/&break;andisa01/Arietta2021_Forestry.git. Due to the large file sizes, raw images are available upon request to the author.

Acknowledgements

I would like to thank Vince Mow for access to Rockstock property and Yale University for access to Yale Preserve. I thank Dr David Skelly, Logan Billet, Dahn-Young Dong, Dr Marlyse Duguid, Dr Jonathan Richardson and Dr Craig Brodersen for providing thoughts on the methods and manuscript.

Conflict of interest statement

The author declares no conflicts of interest.

Funding

Yale Institute for Biospheric Studies and the Kohlberg-Donohoe Research Fellowship.

References

Alvernini, A., Fares, S., Ferrara, C. and Chianucci, F. 2018 An objective image analysis method for estimation of canopy attributes from digital cover photography. *Trees* **32**, 713–723.

Anderson, M.C. 1964 Studies of the woodland light climate I. The photographic computation of light condition. *J. Ecol.* **52**, 27–41.

Barbero-García, I., Cabrelles, M., Lerma, J.L. and Marqués-Mateu, Á. 2018 Smartphone-based close-range photogrammetric assessment of spherical objects. *Photogrammetric Record, The* **33**, 283–299.

Bates, D., Mächler, M., Bolker, B. and Walker, S. 2015 Fitting linear mixed-effects models using lme4. *J. Stat. Software* **67**, 1–48.

Beckschäfer, P., Seidel, D., Kleinn, C. and Xu, J. 2013 On the exposure of hemispherical photographs in forests. *iForest* **6**, 228–237.

Beckschäfer, P. (2015) *Hemispherical_2.0: Batch Processing Hemispherical and Canopy Photographs with ImageJ-User Manual*. doi: 10.13140/RG.2.1.3059.4088.

Bianchi, S., Cahalan, C., Hale, S. and Gibbons, J.M. 2017 Rapid assessment of forest canopy and light regime using smartphone hemispherical photography. *Ecol. Evol.* **7**, 10556–10566.

Brown, M. and Lowe, D.G. 2007 Automatic panoramic image stitching using invariant features. *Int. J. Comput. Vision* **74**, 59–73.

Brown, P.L., Doley, D. and Keenan, R.J. 2000 Estimating tree crown dimensions using digital analysis of vertical photographs. *Agric. For. Meteorol.* **100**, 199–212.

Chen, J.M. and Black, T.A. 1992 Defining leaf area index for non-flat leaves. *Plant Cell Environ.* **15**, 421–429.

Downloaded from https://academic.oup.com/forestry/advance-article/doi/10.1093/forestry/cpab034/6320703 by Yale University Law School user on 17 July 2021

Chen, J.M. and Cihlar, J. 1995 Plant canopy gap-size analysis theory for improving optical measurements of leaf-are index. *Appl. Optics* **34**, 6211–6222.

Chianucci, F. 2020 An overview of in situ digital canopy photography in forestry. *Can. J. For. Res.* **50**, 227–242.

Chianucci, F. and Cutini, A. 2012 Digital hemispherical photography for estimating forest canopy properties: Current controversies and opportunities. *iForest - Biogeosciences and Forestry* **5**. 10.3832/ifor0775-005.

Chianucci, F., Zou, J., Leng, P., Zhuang, Y. and Ferrara, C. 2019 A new method to estimate clumping index integrating gap fraction averaging with the analysis of gap size distribution. *Can. J. For. Res.* **49**, 471–479.

Díaz, G.M., Negri, P.A. and Lencinas, J.D. 2021 Toward making canopy hemispherical photography independent of illumination conditions: A deep-learning-based approach. *Agric. For. Meteorol.* **296**, 108234.

Fangi, G. and Nardinocchi, C. 2013 Photogrammetric processing of spherical panoramas. *Photogrammetric Record, The* **28**, 293–311.

Fastie, C.L. (2010) Estimating stand basal area from forest panoramas. In *Proceedings of the Fine International Conference on Gigapixel Imaging for Science*, Fine International Conference on Gigapixel Imagingfor Science, Carnegie Mellon University, pp. 1–7. Available at: https://doi.org/10.1184/R1/6709391.v1.

Frazer, G.W., Canham, C.D. and Lertzman, K.P. (1999) *Gap Light Analyzer (GLA): Imaging software to extract canopy structure and gap light transmission indices from true-color fisheye photographs, users manual and documentation*. Simon Fraser University, Burnaby, British Columbia. Available at: http://rem-main.rem.sfu.ca/downloads/Forestry/GLAV2UsersManual.pdf.

Frazer, G.W., Trofymow, J.A. and Lertzman, K.P. (1997) *A Method for Estimating Canopy Openness, Effective Leaf Area Index, and Photosynthetically Active Photon Flux Density Using Hemispherical Photography and Computerized Image Analysis Techniques*. BC-X-373. Pacific Forestry Centre, Victoria, British Columbia, Canada. Available at: http://citeseerx.ist.psu.edu/viewdoc/download?doi=10.1.1.477.483&rep=rep1&type=pdf.

Glatthorn, J. and Beckschäfer, P. 2014 Standardizing the protocol for hemispherical photographs: Accuracy assessment of binarization algorithms. *PLoS One* **9**, e111924.

Gonsamo, A., D'odorico, P. and Pellikka, P. 2013 Measuring fractional forest canopy element cover and openness - definitions and methodologies revisited. *Oikos* **122**, 1283–1291.

Grotti, M., Calders, K., Origo, N., Puletti, N., Alivernini, A., Ferrara, C., *et al.* 2020 An intensity, image-based method to estimate gap fraction, canopy openness and effective leaf area index from phase-shift terrestrial laser scanning. *Agric. For. Meteorol.* **280**, 107766.

Gunturk, B.K. 2017 Super-resolution imaging. In *Computational Photography: Methods and Applications*. R., Lukac (ed.). CRC Press, Boca Raton, Florida, USA, pp. 175–208.

Halverson, M.A., Skelly, D.K., Kiesecker, J.M. and Freidenburg, L.K. 2003 Forest mediated light regime linked to amphibian distribution and performance. *Oecologia* **134**, 360–364.

Ignatov, A., Kobyshev, N., Timofte, R., Vanhoey, K. and Van Gool, L. 2017 DSLR-quality photos on mobile devices with deep convolutional networks. In *Proceedings of the IEEE International Conference on Computer Vision (ICCV)*, 2017. pp. 3277–3285. *arXiv [cs.CV]*. Available at: http://arxiv.org/abs/1704.02470 (accessed on 07 September, 2017), preprint: not peer reviewed.

Jennings, S.B., Brown, N.D. and Sheil, D. 1999 Assessing forest canopies and understorey illumination: Canopy closure, canopy cover and other measures. *Forestry* **72**, 59–74.

Li, X. and Ratti, C. 2019 Mapping the spatio-temporal distribution of solar radiation within street canyons of Boston using Google Street View panoramas and building height model. *Landscape Urban Plann.* **191**, 103387.

Luhmann, T. 2004 A historical review on panorama photogrammetry. *Int. Arch. Photogramm. Remote Sens. Spat. Inform. Sci.* **34**, 8.

Lukac, R. 2017 *Computational Photography: Methods and Applications*. CRC Press, Boca Raton, Florida, USA.

Lu, M.-K., Lam, T.Y., Perng, B.H. and Lin, H.T. 2019 'Close-range photogrammetry with spherical panoramas for mapping spatial location and measuring diameters of trees under forest canopies'. *Can. J. For. Res.* **49**, 865–874.

Macfarlane, C. 2011 Classification method of mixed pixels does not affect canopy metrics from digital images of forest overstorey. *Agric. For. Meteorol.* **151**, 833–840.

Macfarlane, C., Ryu, Y., Ogden, G.N. and Sonnentag, O. 2014 Digital canopy photography: Exposed and in the raw. *Agric. For. Meteorol.* **197**, 244–253.

Origo, N., Calders, K., Nightingale, J. and Disney, M. 2017 Influence of levelling technique on the retrieval of canopy structural parameters from digital hemispherical photography. *Agric. For. Meteorol.* **237-238**, 143–149.

Parker G.G. 1995 Structure and microclimate of forest canopies. In *Forest Canopies*. G.G. Parker, M.D. Lowman and N.M. Nadkarni (eds). Academic Press, San Diego, pp. 73–106.

Prewitt, J.M.S. and Mendelsohn, M.L. 1966 The analysis of cell images. *Ann. N. Y. Acad. Sci.* **128**, 1035–1053.

Promis, A. 2013 Measuring and estimating the below-canopy light environment in a forest. A review. **19**, 139–146.

R Core Team. (2019) *R: A Language and Environment for Statistical Computing*. Vienna, Austria: R Foundation for Statistical Computing. Available at: https://www.R-project.org/.

Rich, P.M. 1990 Characterizing plant canopies with hemispherical photographs. *Remote Sens. Rev.* **5**, 13–29.

Stenberg, P., Linder, S., Smolander, H. and Flower-Ellis, J. 1994 Performance of the LAI-2000 plant canopy analyzer in estimating leaf area index of some scots pine stands. *Tree Physiol.* **14**, 981–995.

Szeliski, R. and Shum, H.-Y. (1997) Creating full view panoramic image mosaics and environment maps, In *Computer Graphics (SIGGRAPH'97), 31(Annual Conference Series)*. ACM Press/Addison-Wesley Publishing Co., USA, pp. 251–258.

Tichý, L. (2016) 'Field test of canopy cover estimation by hemispherical photographs taken with a smartphone', *J. Veg. Sci.*. Edited by B. Collins, **27**, 427–435.

Yan, G., Hu, R., Luo, J., Weiss, M., Jiang, H., Mu, X., *et al.* 2019 Review of indirect optical measurements of leaf area index: Recent advances, challenges, and perspectives. *Agric. For. Meteorol.* **265**, 390–411.

Zhang, Y., Chen, J.M. and Miller, J.R. 2005 Determining digital hemispherical photograph exposure for leaf area index estimation. *Agric. For. Meteorol.* **133**, 166–181.

Downloaded from https://academic.oup.com/forestry/advance-article/doi/10.1093/forestry/cpab034/6320703 by Yale University Law School user on 17 July 2021